



Iron oxide mineralogy in late Miocene red beds from La Gloria, Spain: rock-magnetic, voltammetric and Vis spectroscopy analyses

T. Grygar^{a,*}, J. Dědeček^b, P.P. Kruiver^c, M.J. Dekkers^c,
P. Bezdička^a, O. Schneeweiss^d

^a*Institute of Inorganic Chemistry, Academy of Sciences of Czech Republic, Řež 250 68, Czech Republic*

^b*J. Heyrovský Institute of Physical Chemistry, Dolejškova 8, 180 00 Prague 8, Czech Republic*

^c*Utrecht University, Paleomagnetic Laboratory, "Fort Hoofddijk", Budapestlaan 17, 3584 CD Utrecht, The Netherlands*

^d*Institute of Physics of Materials, ASCR, Žitkova 22, 616 62 Brno, Czech Republic*

Received 26 March 2002; accepted 20 January 2003

Abstract

Free ferric oxides of a red bed series were analyzed by rock-magnetic techniques (IRM component analysis) and by two less traditional methods: visible spectroscopy and voltammetry. All three methods have low limits of detection, making them suited for this type of analysis. The red bed samples studied contained clay minerals, quartz, and calcium carbonate as major constituents. Free Fe oxides occurred at a concentration of 0.3–2.1%, i.e. in the majority of the samples below the detection limit of X-ray powder diffraction. The combination of the employed analytical techniques enabled to characterize the mineralogy of free ferric oxides and to estimate the ratio of goethite and to hematite. This ratio changes substantially within the section that probably indicates paleoclimatic changes.

© 2003 Elsevier Science B.V. All rights reserved.

Keywords: Fe oxides; Goethite; Hematite; Red beds; Voltammetry; Diffuse-reflectance spectroscopy

1. Introduction

The relationship between the mineralogy of ferric oxides in soils and the soil-forming environment is a traditional topic in soil science (Schwertmann and Taylor, 1989; Cornell

* Corresponding author. Fax: +420-2-20941502.

E-mail address: grygar@iic.cas.cz (T. Grygar).

and Schwertmann, 1996). From the properties of these ferric oxides paleoclimatic interpretations may be inferred along similar lines as clay minerals (Singer, 1980). In particular, the goethite to hematite ratio is considered to be a good parameter to reconstruct the conditions of Fe oxide formation. Goethite and hematite are the most thermodynamically stable ferric oxides in oxic soils and sediments, and their ratio depends primarily on the parent minerals and on the activity of water during their formation (Trolard and Tardy, 1987). In soils, the transformation rate of ferric oxide due to seasonal cycling, and the reducing and complexing activity of organic substances are important parameters as well (Cornell and Schwertmann, 1996). Due to the high activation energy of the reaction



the goethite-to-hematite ratio remains stable for very long periods unless redox or dissolution–re-precipitation reactions convert these phases.

XRD analysis of clay minerals is fairly laborious (e.g. Moore and Reynolds, 1989) and is limited by the comparatively high limit of detection of the XRD technique. The diagnostic power of other techniques that make use of their dehydration or decomposition temperatures (e.g. thermogravimetric analysis) is not always large, in particular when dealing with low concentrations, the rule in natural samples. Mineral-magnetic techniques that are designed for the analysis of magnetic iron oxides are very sensitive. The same applies to voltammetry of microparticles and diffuse reflectance spectroscopy in the visible light band (Vis diffuse reflectance spectroscopy) as we will show here. Thus, when utilizing these techniques, tedious pre-concentration procedures can be avoided, a distinct analytical advantage.

The identification of ferric oxides in soils, however, is by no means trivial because they often are fine-grained, and comparatively poorly crystalline, in addition to the commonly occurring low concentrations. Evidently, this limits the application of more classical mineralogical techniques like XRD and Mössbauer spectroscopy. With the notable exception of highly weathered lateritic soils, the free ferric oxides are commonly present in concentrations of <2%, that is close to or below the XRD detection limit. Goethite, in particular, cannot be detected in low concentration, because it is frequently less crystalline than hematite and hence its XRD diffraction peaks are broader.

Recently, two new methods are proposed that are about one order of magnitude more sensitive than XRD, i.e. with a limit of detection of ca. 0.1% for free iron oxides in soils and sediments. These methods are diffuse reflectance spectroscopy in the visible region (Vis DRS; Malengreau et al. 1994, 1996, 1997; Scheinost et al. 1998, Scheinost and Schwertmann, 1999) and voltammetry of microparticles (VMP; Grygar and van Oorschot, 2002; van Oorschot et al., 2001). Vis spectroscopy of Fe(III) ions is based on the sensitivity of the energy of d–d electronic transitions of Fe ions to their nearest surrounding, i.e. to the ligand field strength and geometry. Thus, Vis spectra of Fe ions are phase-specific (Sherman and Waite 1985; Scheinost et al. 1998; Scheinost and Schwertmann, 1999). VMP is an electrochemical method and reflects the reactivity of iron oxide particles to reductive dissolution and therefore is specific to phase composition and to grain size and crystallinity (Grygar, 1998). Both methods are relative and require an internal standard or reference compounds to obtain absolute values.

For VMP, the internal standard technique was recently explored by Grygar and van Oorschot (2002) and van Oorschot et al. (2001). VMP appeared to be very sensitive but some samples were rather difficult to interpret because of broad so-called voltamperometric (voltammetric) curves.

Unfortunately, traditional mineralogical techniques with comparable low limits of detection to further test VMP and DRS are non-existent. To contribute to the further quantification of both VMP and DRS, we therefore compare both methods to each other. As an additional check, the interpretation is constrained by the total Fe content and the magnetic properties of the samples. The sample set comprises a series of continental red bed type sediments from the La Gloria section (Spain) of Miocene age (Krijgsman et al., 1996) that have recently been minutely characterized by mineral-magnetic methods (Kruiver et al., 2003). Moreover, a pilot set yielded encouraging results when treated with VMP (van Oorschot et al., 2001).

2. Methods

2.1. Determination of free ferric oxides

Free ferric oxides were determined by the digestion of samples in 25 vol.% acetic acid with 0.04 M $\text{NH}_2\text{OH}\cdot\text{HCl}$ according to Tessier et al. (1979). Dissolved Fe was determined by atomic absorption spectroscopy (AAS; Zeiss 3, Carl-Zeiss Jena, Germany, flame atomization).

2.2. Vis diffuse reflectance spectroscopy

Diffuse reflectance spectroscopy in the visible region (Vis DRS) was employed for the identification and quantification of Fe(III) species in the samples. Spectra of homogenized powdered samples were recorded using a Perkin-Elmer Lambda 19 UV–Vis–NIR spectrometer equipped with a ‘praying mantis’ for collecting scattered light from powdered samples. Spectra were recorded in the region from 200 to 900 nm with 1-nm increments in double beam mode and against BaSO_4 as a reference. The reflectance of light scattering of a powdered sample is not proportional to the concentration of absorbing species. That is why the remission function $F(R_\infty)$, is used; it is defined by the Schuster–Kubelka–Munk equation:

$$F(R_\infty) = \frac{(1 - R_\infty)^2}{2R_\infty}$$

where R_∞ is the diffuse reflectance from a semi-infinite layer). The signal noise was removed by application of a Fourier filter (cross 5 points).

The octahedrally coordinated Fe(III) ions exhibit the strongest d–d absorption band around 500 nm ($20,000 \text{ cm}^{-1}$), which corresponds to the electron pair transition (EPT), (${}^4\text{T}_1 + {}^4\text{T}_1$) \leftarrow (${}^6\text{A}_1 + {}^6\text{A}_1$) (transition denotation according to Sherman, 1985; Sherman and Waite, 1985; Scheinost et al., 1998). Moreover, this transition is observable for all ferric

oxides. Therefore, the estimation and characterization of Fe(III) species in the samples was focussed on this region of the spectra. The wavenumber of the Fe(III) EPT transition in hematite significantly differs from corresponding transitions of other Fe oxides (Scheinost et al., 1998). However, it is necessary to point out here that any of the d–d transition reported for Fe(III) does not distinguish goethite from other Fe oxides (ferrihydrite, lepidocrocite, maghemite, etc.).

The Fe(III) EPT bands of individual oxides are overlap partly. For the separation of overlapping bands, decomposition of the Vis spectra into Gaussian curves is commonly used. However, this decomposition fails when there is a significant difference in the intensity of overlapping bands, as in Fe oxides, of which the EPT bands are superimposed on the tail of the much stronger Fe(III) charge transfer (CT) bands in the UV region (Fig. 1). In this case, analysis of the second derivative mode of the spectra, which suppresses the influence of the dominant CT bands, gives more appropriate results for the weaker d–d bands. Both approaches were used in the present work. Data processing was carried out

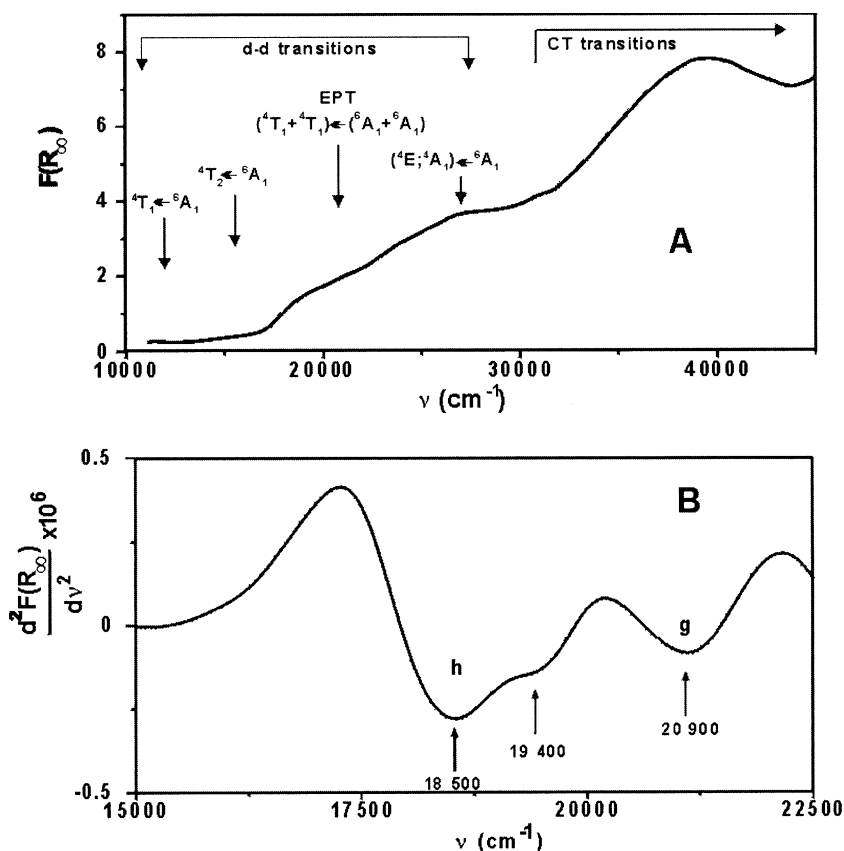
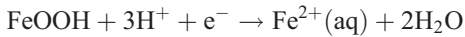
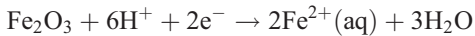


Fig. 1. (A) Vis DRS for the full range. The electron transition bands are denoted according to Scheinost et al. (1998) and Sherman and Waite (1985). (B) Vis DRS in the second derivative mode for wavenumber 15,000 to 22,500 cm^{-1} .

with the help of the curve fitting module of Microcal Origin 4.1 software (Microcal Software, USA).

2.3. Voltammetry of microparticles

Semi-quantitative voltammetric determination of ferric oxides was described by Grygar and van Oorschot (2002). VMP is based on reductive (cathodic) dissolution of Fe_2O_3 or FeOOH via:



The sample is mechanically deposited on the surface of a paraffin-impregnated graphite electrode and immersed into a carefully degassed acetic acid–sodium acetate buffer (0.2 M total acetate, 1:1 acid to acetate). A Pt plate was used as a counter electrode, and a saturated calomel electrode (SCE) as reference electrode. The measurements were performed under N_2 atmosphere to suppress the background current due to oxygen reduction on the working electrode. Two scans were measured between the open-circuit potential (ca. +0.2 V vs. SCE) to –1.15 V vs. SCE at a scan rate of 4 mV/s. The second scan was subtracted from the first one to deduce the net signal of the Fe-oxide reduction to eliminate the otherwise large background current. To discriminate between goethite and hematite, a small portion of samples was heated to 320 °C to convert goethite to more reactive poorly crystalline hematite of which the voltammetric peak is shifted by ca. 200 mV to more positive values. After this heating, the peak of the original hematite does not change (Grygar and van Oorschot, 2002). The goethite to hematite ratio was estimated from the charges (areas) of the corresponding voltammetric peaks. The concentration of ferric oxides was estimated from the comparison of the area of their voltammetric peaks in the samples and that of a Mn oxide that is added in a known amount as internal standard (Grygar and van Oorschot, 2002; van Oorschot et al., 2001).

2.4. Isothermal remanent magnetization curves

Acquisition curves of isothermal remanent magnetisation (IRM) were determined to characterize magnetic properties of the magnetic minerals. IRM acquisition curves were shown to have a cumulative log-Gaussian shape (Robertson and France, 1994). Therefore, each remanent magnetic component can be described by its (i) saturation IRM (SIRM), (ii) the field value at which half of the SIRM has been reached, $B_{1/2}$, and (iii) the dispersion of the distribution, DP (Robertson and France, 1994; Kruiver et al., 2001). The SIRM is a measure of the concentration of the magnetic mineral, while $B_{1/2}$ and DP describe the switching field distribution of the grain ensemble. At room temperature, the saturation magnetizations of magnetite (Fe_3O_4), hematite (Fe_2O_3) and goethite ($\alpha\text{-FeOOH}$) are 90–92, 0.2–0.4, and 0.01–0.1 A m²/kg, respectively. Therefore, from a magnetic viewpoint, magnetite is almost always dominant in the magnetic signal. Hematite and goethite have different magnetic coercivities or switching field distributions. Within each mineral,

however, their variation can be large and both minerals show an overlap in their coercivity. Only when magnetite is absent, or when the relative contributions of hematite or goethite compared to that of magnetite are large, hematite and goethite can be detected individually in samples with mixed magnetic mineralogy.

2.5. Mössbauer spectroscopy

^{57}Fe Mössbauer spectra were taken at room temperature in a transmission geometry. The velocity scale was calibrated using a pure α -iron foil. The program package CONFIT (Žák, 1999) was used for the spectra processing to calculate atomic fractions I (intensities, subspectrum areas) of the spectrum components and their hyperfine field parameters: hyperfine induction B_{hf} , isomer shift δ , and quadrupole splitting σ . Isomer shifts are given relative to α -iron at room temperature.

3. Samples

Samples were taken from a distal alluvial fan in the La Gloria section (NE Spain) of late Miocene age. The sediments have a distinctly red color, indicative of pigmentary hematite. The bottom of the section consists of a regular alternation of caliche and red clay beds. Via a bright yellow hydromorphous layer and brown clays, the lithology grades into lacustrine limestones. The part of the section studied here consists of a 14-m thick succession of caliches and red clays, the hydromorphous layer (~ 2 m) and the brown clays on top of it

Table 1
Integral intensities (absorbance $\times 10^4$) of the second order derivative of DRS in the samples studied

Sample	Stratigraphic level (m)	Lithology	Goethite (21,000 cm^{-1})	Hematite (18,500 cm^{-1})	Fe(III) in clays (19,500 cm^{-1})
GLO3A	0.43	caliche	2.00	1.60	3.20
GLO7A	0.65	red clay	2.30	2.80	4.00
GLO10A	0.99	caliche	1.80	1.90	3.60
GLO14A	1.40	red clay	1.90	1.90	3.60
GLO17A	1.82	caliche	2.80	2.60	4.40
GLO38	4.67	dark red clay	3.30	3.30	5.50
GLO43A	5.91	caliche	4.00	4.80	7.50
GLO46	6.32	dark red clay	3.60	4.00	7.20
GLO50A	7.24	caliche	3.30	4.10	4.80
GLO84	12.02	dark red clay	4.10	3.70	7.10
GLO92	13.19	caliche	2.90	2.10	3.70
GLO97	13.83	dark red clay	7.90	3.80	8.80
GLO102	14.40	caliche	5.50	0.70	4.60
GLO108	15.04	hydromorphous layer	3.20	0.05	1.50
GLO110	15.27	hydromorphous layer	7.20	0.05	5.70
GLO117	16.09	hydromorphous layer	0.90	0	0.20
GLO122	17.00	brown clay	4.90	1.20	3.60
GLO124	18.45	caliche	1.80	1.30	2.50
GLO128	20.75	brown clay	3.30	2.80	2.20
GLO130	22.20	brown clay	1.60	0.70	1.50

(~ 6 m). Samples were taken with an average sampling space of ~ 13 cm. For the present study, 20 samples were selected for a comparison between rock-magnetic, voltammetric and Vis DRS analyses. The general characterization of the samples is given in Table 1.

Two samples of standard clay minerals, palygorskite (PF1-1, Gadsden County, FL, USA) and poorly ordered kaolinite (KGa-2, Warren County, GA, USA), were used as reference compounds for DRS. The palygorskite contains 2.98% total Fe₂O₃ and 0.40% total FeO, the kaolinite 0.98% total Fe₂O₃ and 0.15% total FeO. XRD analysis showed that the two clay minerals do not contain a detectable amount of free ferric Fe(III) oxides.

4. Results

4.1. Vis absorption spectra

The Vis spectroscopy is generally not limited by the varying particle size of the target compounds, neither from the side of nanocrystalline solids, nor from the side of coarse grains. Spectroscopy can hence be interpreted in terms of the presence or concentration of individual phases, not from a granulometric point of view.

The absorption spectra of the samples (Fig. 1A) exhibit a strong absorption band in the UV region with a maximum at ca. 40,000 cm⁻¹, weak bands at ca. 25,000 and 20,000 cm⁻¹, and barely discernable bands at ca. 14,000 and 11,000 cm⁻¹. The absorption band at 40,000 cm⁻¹ corresponds to the Fe–O charge transfer (CT) (together with CT bands of other sample components), the bands at 25,000, 20,000, 14,000 and 11,000 cm⁻¹ to the (⁴E; ⁴A₁) ← ⁶A, (⁴T₁ + ⁴T₁) ← (⁶A₁ + ⁶A₁) and ⁴T₂ ← ⁶A₁, ⁴T₁ ← ⁶A₁ d–d transitions of Fe(III), respectively (Sherman, 1985; Sherman and Waite, 1985). The EPT bands seem to be most appropriate for the characterization of Fe(III) oxides in soils. The bands at 14,000 and 11,000 cm⁻¹ unfortunately are too weak not only for quantitative, but also for qualitative characterization of the samples (also when expressed as their second derivative). The band at 25,000 cm⁻¹ exhibits the highest intensity from all d–d Fe(III) bands, but there is a strong overlap of absorption bands corresponding to a great variety of Fe(III) oxides, including hematite, goethite, and ferrihydrite (Scheinost et al., 1998). Thus, the EPT bands allow discrimination of hematite from other Fe(III) oxides but cannot be used for additional diagnostic purposes. To enhance the diagnostic power, the absorption spectrum in the range 15,000–30,000 cm⁻¹ (covering the Fe(III) EPT range) is decomposed into Gaussian bands.

Three bands with maxima at 18,500, 19,400 and 21,000 cm⁻¹ are present in the spectra or the red bed samples; they change to minima at the same positions in the second derivative spectra (Fig. 1B). Their individual areas and, moreover, also their ratio differs for individual samples. This indicates the presence of three distinct species containing octahedrally coordinated Fe(III) ions. The band at 18,500 cm⁻¹ can be attributed to d–d EPT of Fe(III) in hematite, and that at 21,000 cm⁻¹ to the same transition in goethite (Sherman and Waite, 1985; Malengreau et al., 1994; Scheinost et al., 1998). The band at 19,400 cm⁻¹ was not reported for Fe(III) oxides, but Fe(III) bearing clay minerals absorb in that region (e.g. montmorillonite, Bishop et al., 1993; Sherman, 1985). In the two

‘reference’ clay minerals, that band at ca. $19,400\text{ cm}^{-1}$ was dominant. More details on absorption bands of Fe(III) octahedral species in several other clay minerals is reported elsewhere (Grygar et al., 2002). Malengreau et al. (1994) observed an absorbing species with a maximum at $20,100\text{ cm}^{-1}$ in kaolinite KGa-2 after dithionite–citrate–bicarbonate bleaching and attributed it to akaganeite/ferrihydrate, rather surprising with respect to the reactivity of these oxides in reductive dissolution. Generally, Vis spectra of Fe ions in various minerals have not been fully described.

4.2. Second derivative mode of Vis absorption spectra

The areas of the three diagnostic bands (two EPT, one unidentified, cf. Fig. 1B) were used as a measure of the band intensities (Table 1). The intensity ratio of the band at $19,400\text{ cm}^{-1}$ to the other two bands substantially varies within the sample set ($I_{18,500}/I_{19,400} \approx 0\text{--}1.3$, $I_{21,000}/I_{19,400} \approx 0.5\text{--}4.5$). Noise removal by a Fourier filter seems to be more appropriate for the evaluation of the spectra than application of a cubic spline fitting (applied by Malengreau et al., 1996; Scheinost et al., 1998). In contrast to the cubic spline fitting, the Fourier filter does not alter the shape of fitted curves and does not suppress small shoulders in the spectra corresponding to the low intensity bands.

Thus, the band at $19,400\text{ cm}^{-1}$ cannot be attributed to either of the single species characterized by the bands at $18,500$ and $21,000\text{ cm}^{-1}$ and must represent some other

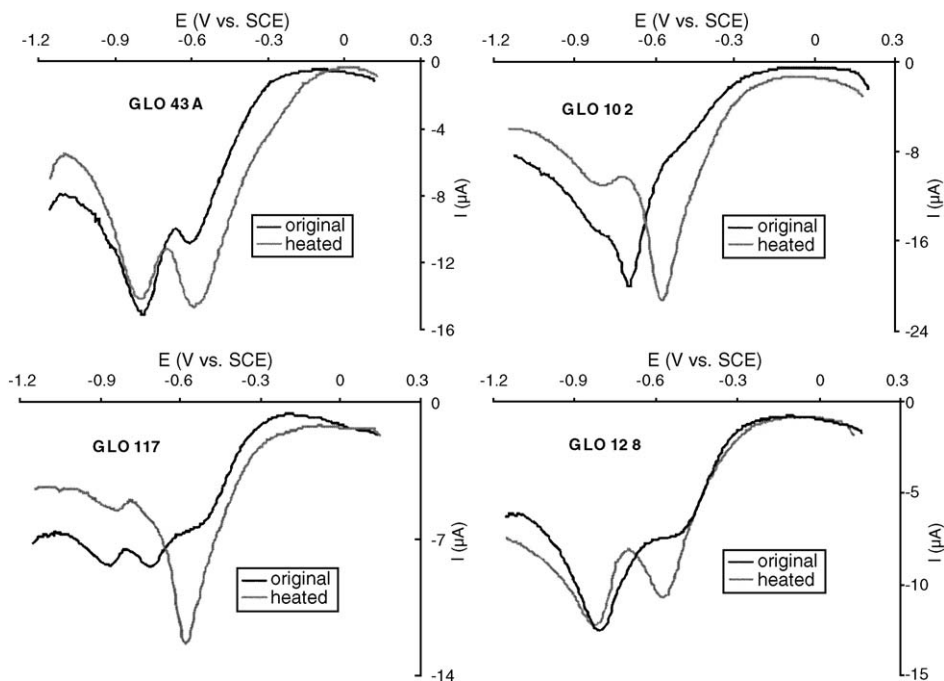


Fig. 2. Examples of voltammetric curves of four samples: original, and after heating at $320\text{ }^{\circ}\text{C}$ to discriminate between hematite and goethite. Difference between first and second scans are plotted.

form of octahedrally or tetrahedrally coordinated Fe(III) ions. Because of the two reference clay minerals, we relate the band at $19,400\text{ cm}^{-1}$ to octahedral Fe(III) in clay minerals. This is supported by the presence of illite in the samples (Krijgsman et al., 1996; Kruiver, 2001); illite can contain a significant amount of substituted ferric iron.

4.3. Voltammetry of microparticles

Voltammetry of microparticles is generally able to detect fine grained Fe oxides, approximately below 1–10 μm . The shift of peak potentials is about 60–100 mV per a decade of particle sizes, but with very large particles (in order of magnitude $>1\ \mu\text{m}$) the voltammetric peaks would change to hardly discernible waves at the moderately acid acetate buffer and at the relatively fast scan rates used. The conditions used in this work are hence most suitable to pedogenic Fe oxides.

Voltammetry detects Fe oxides as current peaks. Because the content of Fe oxides in sediments is very low and a carbon working electrode itself has a significant background current, the net signal of Fe oxides was only obtained by subtracting the second scan from the first scan (Grygar and van Oorschot, 2002). The voltammetric curves of the samples GLO43A, 102, 117 and 128 are shown in Fig. 2 as examples. Basically the two peaks

Table 2

Estimated Fe in free oxides (according to Tessier et al., 1979) and goethite fraction in goethite and hematite obtained by voltammetry and spectroscopy

Sample	Fe oxides in XRD pattern	Fe oxides in IRM analysis	Fe _{oxides} , chemical analysis (%)	Fe _{oxides} , VMP (%)	$Q_g/(Q_g+Q_h)$ (VMP)	$I_g/(I_g+I_h)$ (DRS)
GLO3A		m+h	0.82	0.55	0.05	0.56
GLO7A	?h	m+h	0.59	0.6	0.15	0.45
GLO10A		m+h	0.37	0.7	0.10	0.49
GLO14A	?h	m+h	0.33	0.4	0.12	0.50
GLO17A		m+h	0.37	0.4	0.18	0.52
GLO38		m+h	1.21	0.75	0.13	0.50
GLO43A	?g	m+h	0.38	2	0.18	0.45
GLO46	h	m+h	1.23	2.5	0.11	0.47
GLO50A		m+h	0.26	0.7	0.12	0.45
GLO84	?h	m+h	1.09	1.35	0.28	0.53
GLO92		m+h	0.52	0.45	0.14	0.58
GLO97	?h	m+h	2.10	1.9	0.93	0.68
GLO102	g	m+h+g	1.18	2.5	0.89	0.89
GLO108		m+g	1.59	0.4	0.94	0.98
GLO110	g	m+g	1.57	1.4	1.00	0.99
GLO117		m+g	0.52	0.25	0.40	1.00
GLO122	?g	m+h	1.22	1.3	0.73	0.80
GLO124		m+h	0.34	0.55	0.10	0.58
GLO128		m+h	0.63	0.45	0.15	0.54
GLO130		m+h	0.56	0.35	0.50	0.70
Median					0.17	0.55

h = hematite, I = band area, g = goethite, m = magnetite, Q = charge. Bold letters in the last two columns denotes a value above the corresponding median.

Table 3
IRM component analysis

Sample	Strat. l. (m)	Lithology	Component 1 ^a			Component 2		
			SIRM (A/m)	%	B _{1/2} (mT)	SIRM (A/m)	%	B _{1/2} (mT)
GLO3A	0.43	caliche	3.050	60.2	24.0 (11.0–52.5)	2.02	39.8	603 (263–1380)
GLO7A	0.65	red clay	3.530	59.2	23.4 (10.7–51.3)	2.43	40.8	603 (240–1514)
GLO10A	0.99	caliche	3.630	58.2	22.9 (11.0–47.9)	2.61	41.8	603 (263–1380)
GLO14A	1.40	red clay	3.240	61.7	24.5 (11.5–52.5)	2.01	38.3	575 (229–1445)
GLO17A	1.82	caliche	3.730	63.2	21.9 (10.5–45.7)	2.17	36.8	575 (246–1349)
GLO38	4.67	d. red clay	3.730	52.2	25.7 (12.6–52.5)	3.42	47.8	427 (158–1148)
GLO43A	5.91	caliche	2.230	40.0	25.7 (12.3–53.7)	3.35	60.0	537 (209–1380)
GLO46	6.32	d. red clay	3.740	48.4	25.7 (12.6–52.5)	3.99	51.6	501 (200–1259)
GLO50A	7.24	caliche	2.100	42.5	25.1 (11.7–53.7)	2.84	57.5	550 (229–1318)
GLO84	12.02	d. red clay	4.990	56.5	25.7 (12.3–53.7)	3.84	43.5	479 (173–1318)
GLO92	13.19	caliche	1.950	50.4	25.7 (13.2–50.1)	1.92	49.6	525 (195–1412)
GLO97	13.83	d. red clay	2.140	36.3	30.2 (14.1–64.6)	3.65	63.7	501 (200–1259)
GLO102	14.40	caliche	0.190	6.7	42.7 (15.1–120)	1.36	47.9	214 (105–436)
GLO108	15.04	hydr. layer	0.225	33.5	79.4 (26.9–234)			
GLO110	15.27	hydr. layer	0.147	11.3	72.4 (22.9–229)			
GLO117	16.09	hydr. layer	0.064	37.5	55.0 (18.2–166)			
GLO122	17.00	brown clay	0.152	4.6	57.5 (20.0–166)	3.14	95.4	501 (182–1380)
GLO124	18.45	caliche	0.341	17.0	27.5 (11.0–69.2)	1.66	83.0	479 (151–1514)
GLO128	20.75	brown clay	0.775	21.3	32.4 (13.5–77.6)	2.86	78.7	525 (209–1318)
GLO130	22.20	brown clay	0.130	5.5	51.3 (17.8–148)	2.22	94.5	447 (155–1288)
Sample	Strat. l. (m)	Lithology	Component 3					
			SIRM (A/m)	%	B _{1/2} (mT)			
GLO102	14.40	caliche	1.290	45.4	1550 (550–4365)			

Table 3 (continued)

Sample	Strat. l. (m)	Lithology	Component 3		
			SIRM (A/m)	%	$B_{1/2}$ (mT)
GLO108	15.04	hydr. layer	0.446	66.5	4467 (1413–14 125)
GLO110	15.27	hydr. layer	1.150	88.7	2188 (1349–3548)
GLO117	16.09	hydr. layer	0.106	62.5	1660 (977–2818)

^a SIRM=saturation isothermal remanent magnetization; Strat. l.=stratigraphic level; d. red clay=dark red clay; hydr. layer=hydromorphous layer. $B_{1/2}$ =field value at which half of the SIRM is reached, the dispersion is given between brackets (antilog of $B_{1/2}$ – DP and antilog of $B_{1/2}$ + DP). Component 1 is interpreted as magnetite, component 2 as hematite and component 3 as goethite.

characteristic of these red beds are apparent in original (non-heated) samples (labeled C1 and C2 by van Oorschot et al., 2001). The expression of the most negative peak is variable: in GLO43A and GLO128, it is a single peak at ca. -0.8 V, whereas in GLO102 and GLO117, it consists of a double peak at ca. -0.7 V and at ca. -0.85 V. In GLO43A and GLO128, a second peak at ca. -0.6 V is present, this peak is only emerging as a small shoulder in the other two samples. After heating at 320 °C the peak at ca. -0.6 V is enlarged at the expense of the -0.7 V peak. Therefore, we attributed the -0.6 V peak in heated samples to poorly crystalline hematite (that forms on dehydration of the goethite; Grygar and van Oorschot, 2002) and the -0.7 V peak to goethite and hematite and the -0.85 V peak to hematite. From VMP analysis, it appears that goethite is present in virtually all samples, something that is difficult to assess with mineral-magnetic means (see Section 4.4).

Relative ratios of goethite to hematite were obtained by comparing the areas of the peaks before and after heating. Absolute values for the concentration of Fe oxides were obtained in other experiments with known additions of MnO_2 as described in more detail elsewhere (Grygar and van Oorschot, 2002). By combining the relative amount of goethite to hematite and the absolute amount of total Fe in oxides, absolute values of goethite and hematite were calculated and used for comparison with the results of Vis spectroscopy and IRM component analysis. The results of voltammetric analysis are given in Table 2.

4.4. IRM component analysis

IRM component analysis (cf. Table 3) reveals the presence of two components in most red or brown samples (Fig. 3a,d). The low-coercivity component or component 1 ($B_{1/2}$ range ~ 22 – ~ 30 mT) is interpreted as being due to magnetite. The second component has coercivities ($B_{1/2}$ range ~ 450 – ~ 600 mT) that are typical of hematite. In the yellow hydromorphous layer, the second component, now labeled component 3 in Table 3, has an even higher mean coercivity ($B_{1/2}$ range ~ 1.5 – ~ 4.5 T), which points to goethite instead of hematite (Fig. 3b). In one sample (GLO102), located just below the hydromorphous layer, both hematite and goethite can be distinguished magnetically

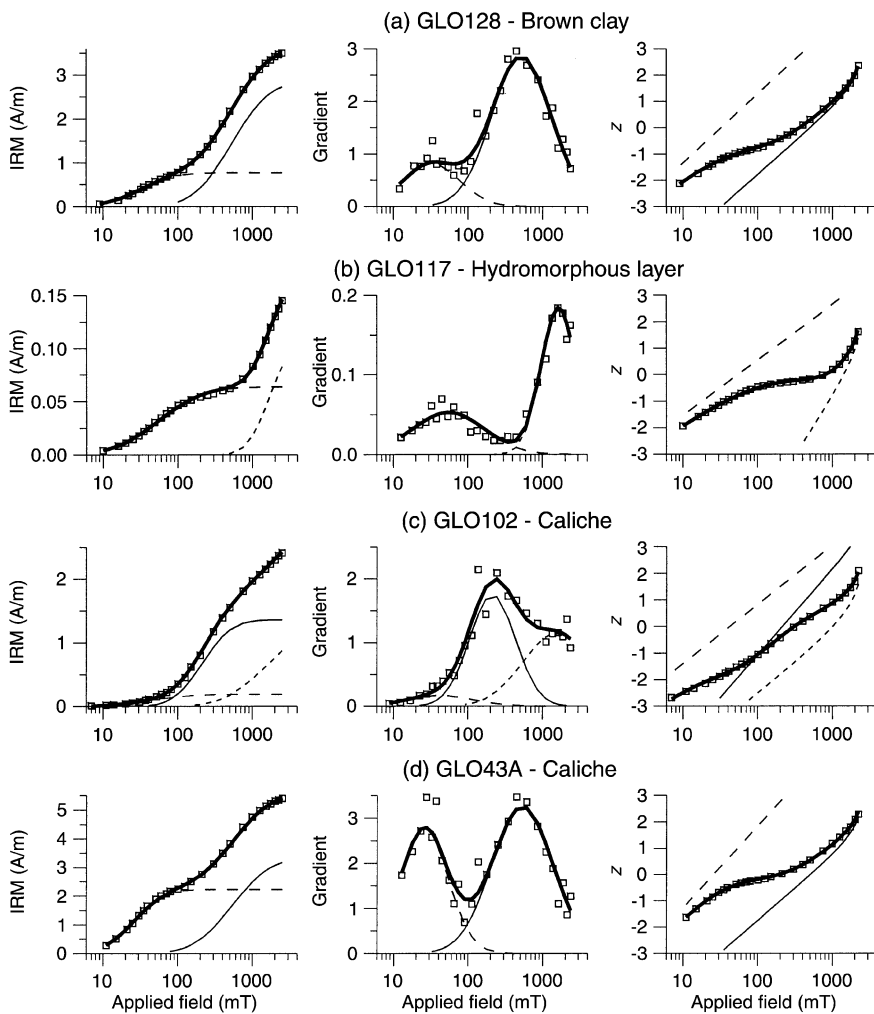


Fig. 3. Examples of IRM acquisition curves and IRM component analysis. Left panels: Linear acquisition plots, central panels: gradient acquisition plots and right panels: standardized acquisition plots. Squares are data points; long dashed line represents magnetite, solid line hematite and short dashed line goethite; bold solid line represents the best-fit sum of components through the data points. GLO43A is representative of the red clays and caliches in the lower part of the section, and contains magnetite (low applied field values) and hematite (intermediate applied field values). GLO102 is just below the hydromorphous layer, and the only sample for which hematite and goethite (high applied field values) could be distinguished magnetically. GLO117 is from the hydromorphous layer, which contains magnetite and goethite. The brown clay sample (GLO128) contains hematite again and relatively minor amounts of magnetite.

(Fig. 3c). It should be noted that the mean coercivity of the hematite in this sample is distinctly lower than that of hematite in the other samples. This may be caused by a finer grain size of the hematite in GLO102. Magnetically, the magnetite component makes up ca. 40–60% of the total remanent magnetization (SIRM) up to the hydro-

morphous layer irrespective of lithology. In molar terms, the magnetite contribution is much lower because of the high SIRM per unit mass ($\sim 45 \text{ A m}^2/\text{kg}$ for single domain (SD) grains) compared to that of hematite ($\sim 0.1 \text{ A m}^2/\text{kg}$ for SD grains) and in particular goethite ($\sim 0.02 \text{ A m}^2/\text{kg}$ for SD grains). In and above that layer, the magnetite contribution distinctly lowers while it becomes magnetically harder ($B_{1/2}$ range $\sim 30 - \sim 80 \text{ mT}$). This points to a finer grain size and/or maghemitized particles. The dispersion (listed in [Table 3](#) as the antilogs of $B_{1/2} - \text{DP}$ and $B_{1/2} + \text{DP}$) becomes larger (DP in logarithmic units increases from ~ 0.32 to ~ 0.45) which would point to maghemitization. The influence of the hydromorphous layer on the hematite properties is subtle. The hematite amounts vary through the section without apparent relation to lithology. Below the hydromorphous layer, in most cases the dispersion DP of the caliches tends to be slightly lower than that of the red clay lithology (DP of caliche ranges $\sim 0.36 - \sim 0.40$ logarithmic units vs. DP of red clay $\sim 0.38 - \sim 0.42$ logarithmic units), while above this layer DP has increased towards a range of $\sim 0.40 - \sim 0.47$ logarithmic units. Intriguingly, in the topmost part of the section starting just below the hydromorphous layer at level GLO102, VMP curves of unheated samples show a broad peak at $\sim -0.45 \text{ V}$ while lower in the section the peak shows up at $\sim -0.60 \text{ V}$. The behaviour of the natural remanent magnetization is suspect in the top part of the section ([Kruiver, 2001](#)).

The total content of free ferric iron oxides varies between 0.3% and 2%. XRD (limit of detection ca. 1%) therefore never revealed magnetite, and hematite and goethite in a few samples only. Because of the limited number of data points in the high-field part of the IRM acquisition curves, goethite and hematite could not be discriminated in by far most red clay and caliche samples. Indication for its presence could be deduced from by another rock-magnetic technique, analysis of first-order-reversal-curves (FORCs) in so-called FORC diagrams ([Pike et al., 1999](#)) that are based on substantially more data points ([Kruiver et al., 2003](#)). The presence of goethite in all samples is confirmed by the VMP and DRS results. Part of the variability of the ‘hematite properties’ could in reality be due to varying goethite amounts.

4.5. Mössbauer spectroscopy

Room temperature Mössbauer spectroscopy ([Table 4](#)) yielded a combined estimate of crystallinity of the Fe oxides and the phase composition in the case of the well-crystalline fraction of hematite and goethite. A well-crystalline magnetically ordered phase, i.e. hematite according to the data given by [Cornell and Schwertmann \(1996\)](#), is undoubtedly responsible for a well-developed sextet with hyperfine fields 47–51 T. A collapsed sextet with hyperfine fields 5–25 T can possibly be attributed to pedogenic goethite. In four of five samples selected for Mössbauer spectroscopy, the major part of ferric ions was present as superparamagnetic (oxides with a particle size in the order of 1–10 nm) or paramagnetic species (e.g. Fe in a clay mineral matrix). Fe oxides are hence mostly present as very small (sub-micrometer) particles that justified application of voltammetry of microparticles. The Mössbauer spectrum of sample GLO110 differed from the four others by prevailing collapsed sextet, and also in GLO122 the area of the collapsed sextet is relatively large. In GLO38, GLO46, and

Table 4
Results of the Mössbauer phase analysis

Sample	Sextets (47–51 T)	Collapsed sextets (5–25 T)	Doublets
GLO38	0.12	–	0.89
GLO46	0.18	0.03	0.79
GLO84	0.14	0.08	0.78
GLO110	–	0.83	0.17
GLO122	0.07	0.21	0.72

The area of individual components are given in dimensionless fractions. The component identification is discussed in the text.

GLO84 the area of the well-developed sextet is larger than that of the collapsed sextet.

5. Discussion

5.1. Evaluation of DRS

Although DRS is based on the processing of electronic absorption spectra in the visible region, it is not simply related to the sample color, which is mainly attributed to the most intense visible absorption band (single-electron transitions, at approximately 25,000 cm^{-1}). As was reported by Malengreau et al. (1994) and Scheinost et al. (1998) and confirmed in this study, the slightly less intense electron-pair transition bands are more suitable for discrimination of ferric oxides presented in sediments, and actually those bands are used in DRS. DRS is able to distinguish more chromophores, even if they are partly overlapped. If for example redness indices were used instead of DRS, the entire complexity of the spectra were reduced to a single value, that would mean irreversible data reduction.

Because specific reflectances for goethite and hematite are not available, only the relative ratio of the band intensity is used in this study to estimate ratios of goethite to hematite. A similar approximation was used by Scheinost et al. (1998), who compared heights of selected second derivative absorption minima and maxima to the results of the quantitative analysis by X-ray diffraction with a very plausible correlation. In fact, the d–d electron pair transitions at $\sim 20,000 \text{ cm}^{-1}$ are more intense in hematite than in goethite due to stronger antiferromagnetic coupling in hematite (Sherman, 1985; Sherman and Waite, 1985). However, the results by Scheinost et al. (1998) proved that the semi-empirical approach to second derivative spectra processing can serve as, at least, a semi-quantitative estimate of the content of Fe oxides.

For the estimate of the relative amount of goethite and hematite, we used the ratio of the intensities of the second derivative absorption bands fitted by Gaussian curves (Table 1). As it is mentioned in Section 4.1, the relatively weak diagnostic d–d transitions are superposed on the very strong charge-transfer bands in the near UV region. Because the ferric oxides content in the red bed samples was very low (by an order of magnitude less than in samples analyzed by Scheinost et al., 1998), fitting the raw (non-derivative) spectra

was hardly possible in some samples. Fitting second derivative spectra was done simultaneously with qualitative evaluation of the raw spectra to check for the reasonability of the procedure.

Surprisingly, during statistical analysis of DRS data we observed a statistically highly significant relationship (Student's *t*-test, 95% significance level) between the intensities of the 19,400, 18,500 and 21,000 cm^{-1} bands, thus between the total amount of free ferric oxides (goethite and hematite) and Fe(III) in clay minerals.

$$I_{19,400} = 0.89 * I_{18,500} + 0.70 * I_{21,000}, \quad r^2 = 0.858 (n = 20)$$

This dependence could be plausible if equilibrium exists between the free ferric oxides responsible for the intensities of the bands at 18,500 and 21,000 cm^{-1} , and substituted Fe(III) in octahedral sites in clay minerals. The underlying central question is the timing of this equilibrium. It may represent equilibrium during early stages in the red bed formation (both free ferric oxides and substituted ferric ions in the clays were formed in certain proportion in the catchment area or during pedogenesis), or a post-depositional equilibrium (solid-state equilibration of free ferric oxides and clay minerals in the sediment). Both processes suggested here merit further investigation because—if substantiated—they may shed light on equilibration between oxides and clay minerals in paleosols that is central to any paleoclimatic interpretation.

5.2. Comparison of DRS, VMP and magnetic properties

The comparison of proxies characteristic of the mineralogical composition of the ferric oxides in the samples studied is summarized in Fig. 4. In Fig. 4A and B, results of Vis spectroscopy and voltammetry are compared. The dependencies are statistically significant, however, the non-zero intercept in the dependence of the goethite absorption band intensity and the goethite content according to voltammetry indicates that there is some source of a systematic error in data interpretation in at least one of these techniques. The non-zero intercept in the comparison of the $g/(g+h)$ ratios obtained by voltammetry and spectroscopy (Fig. 4C) is a direct consequence of this fact. We were not able to identify the source of this systematic error.

In the last two columns of Table 2, $g/(g+h)$ ratios obtained by voltammetry and Vis spectroscopy are compared. The values above the corresponding medians (0.55 in DRS, 0.17 in VMP) are indicated by bold letters. It is obvious that in samples GLO97 to GLO122, the goethite content is increased above the corresponding medians. In these samples (actually except for the boundary samples GLO97 and GLO122), also IRM component analysis indicated the goethite presence.

The SIRM values of component 2 in the IRM component analysis are related to the intensities of the hematite absorption band (Fig. 4D). Neither in that dependence the intercept is equal to 0, but the regression coefficient is statistically significant and hence confirms the interpretation of IRM component analysis.

The individual techniques used are variably sensitive to individual Fe oxides. Rock magnetism is well known to be extremely sensitive to ferrimagnetic phases,

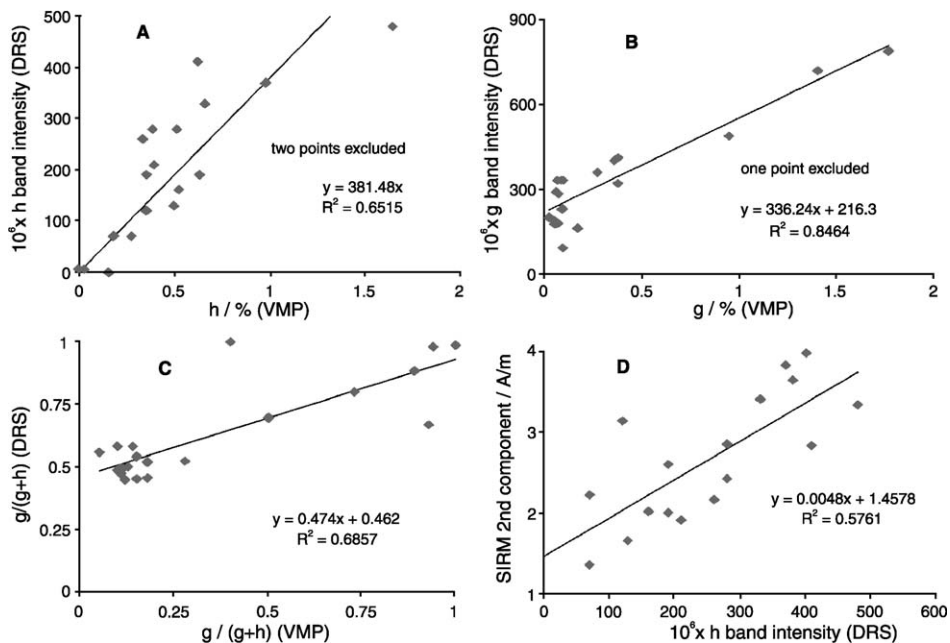


Fig. 4. Comparisons of the mineralogical characteristics obtained by various methods. (A and B) Intensity of Vis spectroscopic bands of hematite (h) and goethite (g), respectively, plotted against the voltammetric estimates of the percentages of these phases. (C) $g/(g+h)$ determined from band intensities in Vis spectroscopy plotted against $g/(g+h)$ obtained by VMP. (D) Percentage of the second SIRM component plotted against the intensity of the hematite Vis spectroscopic band.

magnetite and maghemite. Hematite can also be detected by IRM component analysis, if its content exceeds ca. 0.1%, and goethite is least sensitively detected. We had expected that Vis spectroscopy and voltammetry should be equally sensitive to all Fe(III) oxides. For goethite and hematite—the two ferric oxides present in the largest weight percentage—voltammetry appeared to be more sensitive for the detection of goethite than Vis spectroscopy using the data processing procedure adopted. However, the comparison of the results of both methods indicated the presence of a systematic error as deduced from the non-zero intercepts on either the abscissa or the ordinate.

5.3. Climatic implication

Hematite prevails over goethite in samples GLO3A to GLO92 and at higher stratigraphic levels than GLO124. The opposite is true for samples GLO97 to GLO122, regardless of the lithology of the samples. This dramatic change in ferric oxide pigment composition probably reflects two changes in environmental conditions: to more humid between GLO92 and GLO97 and back to less humid conditions between GLO122 and GLO124.

Acknowledgements

This study was supported in part by the Earth and Life Sciences Division of the Netherlands Science Organization and by the Ministry of Education of the Czech Republic (Project no. LN00A028).

References

- Bishop, J.L., Pieter, C.M., Burns, R.G., 1993. Reflectance and Moessbauer spectroscopy of ferrihydrite–montmorillonite assemblages as Mars soil analog materials. *Geochim. Cosmochim. Acta* 57, 4583–4595.
- Cornell, R.M., Schwertmann, U., 1996. *The Iron Oxides*. VCH, Weinheim.
- Grygar, T., 1998. Phenomenological kinetics of irreversible electrochemical dissolution of metal-oxide micro-particles. *J. Solid State Electrochem.* 2, 127–136.
- Grygar, T., van Oorschot, I.H.M., 2002. Voltammetric identification of pedogenic iron oxides in paleosol and loess. *Electroanalysis* 14, 339–344.
- Grygar, T., Dědeček, J., Hradil, D., 2002. Analysis of low concentration of free ferric oxides in clays by Vis-diffuse reflectance spectroscopy and voltammetry. *Geol. Carpath.* 53, 71–77.
- Krijgsman, W., Garces, M., Langereis, C.G., Daams, R., van Dam, J., van der Meulen, A.J., Augusti, J., Cabrera, L., 1996. A new chronology for the middle to miocene continental record in Spain. *Earth Planet. Sci. Lett.* 142, 367–380.
- Kruiver, P.P., 2001. Unravelling the magnetic record in marine and continental sediments: climatic versus geomagnetic signals. PhD thesis, Utrecht University, *Geologica Ultraiectica*, vol. 210.
- Kruiver, P.P., Dekkers, M.J., Heslop, D., 2001. Quantification of magnetic coercivity components by the analysis of acquisition curves of isothermal remanent magnetisation. *Earth Planet. Sci. Lett.* 189, 269–276.
- Kruiver, P.P., Langereis, C.G., Dekkers, M.J., Krijgsman, W., 2003. Rock-magnetic properties of multi-component natural remanent magnetisation in alluvial red beds (NE Spain). *Geophys. J. Int.* (in press).
- Malengreau, N., Muller, J.-P., Calas, G., 1994. Fe-speciation in kaolins: a diffuse reflectance study. *Clays Clay Miner.* 42, 137–147.
- Malengreau, N., Bedidi, A., Muller, J.P., Herbillon, A.J., 1996. Spectroscopic control of iron oxide dissolution in two ferralitic soils. *Eur. J. Soil Sci.* 47, 13–20.
- Malengreau, N., Weidler, P.G., Gehring, A.U., 1997. Iron oxides in laterites: a combined mineralogical, magnetic, and diffuse reflectance study. *Schweiz. Mineral Petrogr. Mitt.* 77, 13–20.
- Moore, D.M., Reynolds, R.C., 1989. *X-ray diffraction and the identification and analysis of clay minerals*. Oxford Univ. Press. 332 pp.
- Pike, C.R., Roberts, A.P., Verosub, K.L., 1999. Characterizing interactions in fine magnetic particle systems using first order reversal curves. *J. Appl. Phys.* 85, 6660–6667.
- Robertson, D.H., France, D.E., 1994. Discrimination of remanence-carrying minerals in mixtures, using isothermal remanent magnetisation acquisition curves. *Phys. Earth Planet. Inter.* 82, 223–234.
- Scheinost, A.C., Schwertmann, U., 1999. Color identification of iron oxides and hydroxysulfates: use and limitations. *Soil Sci. Soc. Am. J.* 63, 1463–1471.
- Scheinost, A.C., Chavernas, A., Barrón, V., Torrent, J., 1998. Use and limitations of second-derivative diffuse reflectance spectroscopy in the visible to near-infrared range to identify and quantify Fe oxide minerals in soils. *Clays Clay Miner.* 46, 528–536.
- Schwertmann, U., Taylor, R.M., 1989. Iron Oxides. In: Dixon, J.B., Weed, S.B. (Eds.), *Minerals in Soil Environments*. Soil Science Society of America, Madison, WI, USA, pp. 395–406.
- Sherman, D.M., 1985. The electronic structures of Fe³⁺ coordination sites in iron oxides; applications to spectra, bonding, and magnetism. *Phys. Chem. Miner.* 12, 161–175.
- Sherman, D.M., Waite, T.D., 1985. Electronic spectra of Fe³⁺ oxides and oxide hydroxides in the near IR to near UV. *Am. Mineral.* 70, 1262–1269.
- Singer, A., 1980. The paleoclimatic interpretation of clay minerals in soils and weathering profiles. *Earth Sci. Rev.* 15, 303–326.

- Tessier, A., Campbell, P.G.C., Bisson, M., 1979. Sequential extraction procedure for the speciation of particulate trace metals. *Anal. Chem.* 51, 844–851.
- Trolard, F., Tardy, Y., 1987. The Stabilities of gibbsite, boehmite, aluminous goethites and aluminous hematites in bauxites, ferricretes and laterites as a function of water activity, temperature and particle size. *Geochim. Cosmochim. Acta* 51, 945–957.
- van Oorschot, I.H.M., Grygar, T., Dekkers, M.J., 2001. Detection of low concentrations of fine-grained iron oxides by voltammetry of microparticles. *Earth Planet. Sci. Lett.* 193, 631–642.
- Žák, T., 1999. In: Miglierini, M., Petridis, D. (Eds.), *Mössbauer Spectroscopy in Materials Science*. NATO Science Series, 3. High Technology, vol. 66. Kluwer Academic Publishing, Dordrecht, p. 385.